J. Fluid Mech. (2009), *vol.* 620, *pp.* 383–411. © 2009 Cambridge University Press
doi:10.1017/S0022112008004722 Printed in the United Kingdom

Large eddy simulation of a circular jet: effect of inflow conditions on the near field

JUNGWOO KIM AND HAECHEON CHOI†

School of Mechanical and Aerospace Engineering, Seoul National University, Seoul 151-744, Korea

(Received 27 April 2007 and in revised form 22 October 2008)

In the present study, the effects of the jet inflow conditions such as the initial momentum thickness (θ) and background disturbances on the downstream evolution of a circular jet are investigated using large eddy simulation (LES). We consider four different initial momentum thicknesses, $D/\theta = 50$, 80, 120 and 180, and three different Reynolds numbers, $Re_D = U_J D/\nu = 3600$, 10^4 and 10^5, where U_J is the jet inflow velocity and D is the jet diameter. The present study shows that the jet characteristics significantly depend on both the initial momentum thickness and the Reynolds number. For all the Reynolds numbers considered in this study, vortex rings are generated at an earlier position with decreasing initial momentum thickness. In case of a relatively low Reynolds number of $Re_D = 3600$, at smaller initial momentum thickness, early growth of the shear layer due to the early generation of vortex ring leads to the occurrence of large-scale coherent structures in earlier downstream locations, which results in larger mixing enhancement and more rapid increase in turbulence intensity. However, at a high Reynolds number such as $Re_D = 10^5$, with decreasing initial momentum thickness, rapid growth of the shear layer leads to the saturation of the shear layer and the generation of fine-scale turbulence structures, which reduces mixing and turbulence intensity. With increasing Re_θ ($= U_J\theta/\nu$), the characteristic frequency corresponding to the shear layer mode ($St_\theta = f\theta/U_J$) gradually increases and reaches near 0.017 predicted from the inviscid instability theory. On the other hand, the frequency corresponding to the jet-preferred mode ($St_D = fD/U_J$) varies depending on Re_D and D/θ. From a mode analysis, we show that, in view of the energy of the axial velocity fluctuations integrated over the radial direction, the double-helix mode (mode 2) becomes dominant past the potential core, but the axisymmetric mode (mode 0) is dominant near the jet exit. In view of the local energy, the disturbances grow along the shear layer near the jet exit: for thick shear layer, mode 0 grows much faster than other modes, but modes 0–3 grow almost simultaneously for thin shear layer. However, past the potential core, the dominant mode changes from mode 0 near the centreline to mode 1 and then to mode 2 with increasing radial direction regardless of the initial shear layer thickness.

† Email address for correspondence: choi@snu.ac.kr. Also at Center for Turbulence and Flow Control Research, Institute of Advanced Machinery Design, Seoul National University, Seoul 151-744, Korea.

1. Introduction

The jet is a typical flow phenomenon encountered in various engineering applications such as mixing, heating/cooling, printing and propulsion. Especially, the circular jet is a flow commonly observed in many industrial devices. Therefore, a clear understanding of mixing and noise generation mechanism of the circular jet is of practical concern. Also, the initial development of the circular jet is considered as one of the representative free shear flows.

The important features of the jet such as mixing and noise generation are closely associated with the development of turbulence generated from the jet. It has been reported that the jet development is very sensitive to jet inflow conditions characterizing the evolution of the initial shear layer (Bradshaw 1966; Hill, Jenkins & Gilbert 1976), and the mixing and noise generation also significantly depend on them (Mi, Nobes & Nathan 2001; Bogey & Bailly 2005). Therefore, understanding the effect of the jet inflow conditions is critical in predicting and controlling the jet flow.

Crow & Champagne (1971) showed that coherent structures appear past the potential core and have the characteristic frequency called the jet-preferred mode. After this important finding, many studies have shown that turbulent jet flows consist of large-scale coherent structures and fine-scale turbulence motions, and these coherent structures dominate the dynamics and mixing of a jet (see, for example, Yule 1978; Hussain 1983, 1986). Hence, to understand the effect of the jet inflow conditions, their effect on the vortical evolution should be investigated.

Hussain & Zedan (1978*a*, *b*) first systematically investigated the effect of the jet inflow conditions such as the momentum thickness ($D/\theta = 180 - 700$) and disturbances on the jet evolution, where θ is the jet initial momentum thickness (see §2 for the definition of θ) and D is the jet diameter. They found that the distance to reach self-preservation depends on both the initial momentum thickness and the initial disturbance level, but the spread rate, similarity parameter and peak turbulent intensity in the self-preserving region are changed by the initial disturbances more than by the jet momentum thickness. However, the disturbance level used in their study was quite high (about 5% of the jet inflow velocity).

Gutmark & Ho (1983) reported that various values of the jet-preferred-mode frequency in the literature are attributed to different inflow conditions. According to the data summarized by Gutmark & Ho, the jet-preferred-mode frequency normalized by the jet inflow velocity U_J and the jet diameter D has a tendency to approach a constant value of about 0.42 (Drubka 1981) or 0.45 (Kibens 1981) as the Reynolds number becomes large. These studies indicated that the jet-preferred mode or formation of coherent structures is related to the evolution of the shear layer characterized by the jet inflow conditions. However, the detailed relation of the jet inflow conditions to the jet-preferred-mode frequency has not been fully resolved yet.

Russ & Strykowski (1993) investigated the influence of the jet momentum thickness on the jet mixing at Re_D $(= U_J D/\nu) = 10^4$, where ν is the kinematic viscosity. They considered three different values of D/θ (48, 86 and 110) and showed that the jet-centreline velocity for $D/\theta = 48$ decays more slowly than those for larger values of D/θ and less mixing occurs at smaller D/θ. The change of the jet mixing with D/θ is caused by the fact that increasing D/θ promotes the vortex roll-up, giving rise to the decrease of the jet potential core. Stanley & Sarkar (2000) examined the influence of the jet inflow conditions using direct numerical simulation of a planar jet at $Re_H = 3000$, where H is the nozzle width of the planar jet. Similarly to Russ & Strykowski (1993), they reported that the entrainment and jet half-width characterizing the jet mixing increase as the jet initial momentum thickness decreases

or the background disturbance level increases. Bogey & Bailly (2005) investigated the effect of the inflow conditions at $Re_D = 4 \times 10^5$ using large eddy simulation (LES). They also observed that transition to turbulence occurs more rapidly for thinner momentum thickness (i.e. larger D/θ), resulting in the increase of the jet mixing. Therefore, it appears from these studies that the jet mixing has a tendency to increase with decreasing initial momentum thickness. However, the ranges of the inflow conditions considered in the previous numerical studies are quite different from those in the experiments. For example, in Stanley & Sarkar and Bogey & Bailly, the values of D/θ are around 50, but most of the values reported in the experiments are over 100 (Hussain & Zedan 1978*a*, *b*; Russ & Strykowski 1993). As mentioned in Bodony & Lele (2005), the evolution of thick initial shear layer may be quite different from that of thin initial shear layer. Therefore, it should be interesting to see if the results of Stanley & Sarkar and Bogey & Bailly are still valid in the cases of the inflow conditions close to experimental values.

For the reasons mentioned above, our understanding of the effect of the jet inflow conditions remains unclear, although there exist quite a few investigations addressing this issue. Therefore, in the present study, we investigate the effect of the initial momentum thickness of jet inflow velocity on the jet evolution at $Re_D = 3600$, 10^4 and 10^5 using LES. We consider four different jet initial momentum thicknesses, $D/\theta = 50$, 80, 120 and 180. The computational details are described in § 2, where the jet inflow conditions such as the initial momentum thickness and background disturbance are provided. The effects of the jet momentum thickness on the vortical structures and turbulence statistics are presented in § 3.1, followed by a discussion regarding the temporal and spatial instability modes in §§ 3.2 and 3.3, respectively. Finally, conclusions are given in § 4.

2. Computational details

The filtered governing equations of an unsteady incompressible viscous flow for LES are

$$\frac{\partial \tilde{u}_i}{\partial t} + \frac{\partial \tilde{u}_i \tilde{u}_j}{\partial x_j} = -\frac{\partial \tilde{p}}{\partial x_i} + \frac{1}{Re_D}\frac{\partial^2 \tilde{u}_i}{\partial x_j \partial x_j} - \frac{\partial \boldsymbol{\tau}_{ij}}{\partial x_j}, \tag{2.1}$$

$$\frac{\partial \tilde{u}_i}{\partial x_i} = 0, \tag{2.2}$$

where x_i are the coordinates, $\tilde{u}_i$ are the corresponding filtered velocity components, $\tilde{p}$ is the filtered pressure and Re_D denotes the Reynolds number. The subgrid-scale (SGS) stress tensor, $\boldsymbol{\tau}_{ij} = \widetilde{u_i u_j} - \tilde{u}_i \tilde{u}_j$, is modelled using the dynamic SGS model by Germano *et al.* (1991), together with the least-square method suggested by Lilly (1992).

We solve (2.1) and (2.2) in the cylindrical coordinate system using a semi-implicit fractional-step method proposed by Akselvoll & Moin (1996). The computational domain is decomposed into core and outer regions. Within each region only the derivatives in one direction, i.e. the derivatives in the azimuthal direction within the core region and those in the radial direction within the outer region, are treated implicitly, and other derivatives are treated explicitly. The Crank–Nicolson method is used for the implicit terms and a third-order Runge–Kutta method is used for the explicit terms. Also, the second-order central difference scheme is employed for all the spatial derivative terms.

Figure 1 shows the schematic diagram of the computational domain used in this study. Here, x, r and ϕ denote the axial, radial and azimuthal directions, respectively.

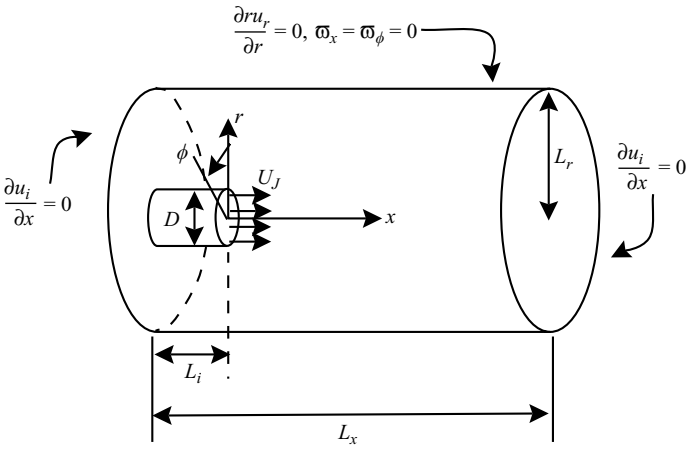

FIGURE 1. Schematic diagram of the computational domain and boundary conditions.

As shown in figure 1, the Neumann condition, $\partial u_i/\partial x = 0$, is imposed on the side of the inlet boundary ($x = -L_i$) and the outflow boundary ($x = L_x - L_i$). At the jet inflow ($x = 0$, $r \leqslant D/2$), a Dirichlet boundary condition is applied and the detail of the jet inflow condition is given in the paragraph below. At the far-field ($r = L_r$), $\partial(ru_r)/\partial r = 0$ and $\omega_x = \omega_\phi = 0$ are given, where $\boldsymbol{\omega} = (\omega_x, \omega_r, \omega_\phi)$ is the vorticity vector. As shown in figure 1, we locate the jet exit inside the computational domain because this configuration allows natural entrainment from the side of inlet boundary ($x = -L_i$). A similar approach was taken by Babu & Mahesh (2004).

As the jet inflow condition, we give a constant velocity U_J in the jet core region and a laminar Blasius profile near the wall (figure 2*a*), as observed in previous experimental studies (Hussain & Zedan 1978*a*; Russ & Strykowski 1993; Cho, Yoo & Choi 1998). We consider four different momentum thicknesses of the boundary layer covering a relatively wide range of shear layer thickness: $D/\theta = 50$, 80, 120 and 180. The jet initial momentum thickness θ is defined as $\int_0^{D/2} \frac{U_x}{U_J}(1 - \frac{U_x}{U_J})|_{x=0}\, \mathrm{d}r$. Here, we used the definition of momentum thickness for planar geometry assuming that the shear layer is thin relative to the jet exit diameter. When we consider the geometry effect, the jet initial momentum thickness may be defined as $\theta^* = \frac{2}{D}\int_0^{D/2} \frac{U_x}{U_J}(1 - \frac{U_x}{U_J})|_{x=0}\, r\, \mathrm{d}r$. Following this definition, $D/\theta^* \approx 57$, 87, 126 and 186, respectively, for $D/\theta = 50$, 80, 120 and 180. The jet evolution should depend on the Reynolds number as well as the initial momentum thickness because both are the critical parameters for the shear layer instability. Therefore, we consider four different Reynolds numbers, $Re_D = 100$, 3600, 10^4 and 10^5, covering both laminar and turbulent jets. LESs are conducted for $Re_D = 3600$, 10^4 and 10^5. When $Re_D \lesssim 10^5$, the jet inflow condition exhibits laminar characteristics, but it becomes turbulent as the Reynolds number is further increased (Crow & Champagne 1971; Zaman 1985).

In most experimental set-ups, background disturbances exist at the jet exit and the jet characteristics are sensitive to a slight change in those disturbances. In the present study, we generate a background disturbance at the jet exit using the method by Lee, Lele & Moin (1992), assuming that the same type of disturbances exists both in the jet core region and inside the laminar boundary layer near the wall. As shown in figure 2(*b*), we construct the background disturbance such that its frequency spectrum consists of the Kolmogorov spectrum in the inertial region and the Pao spectrum

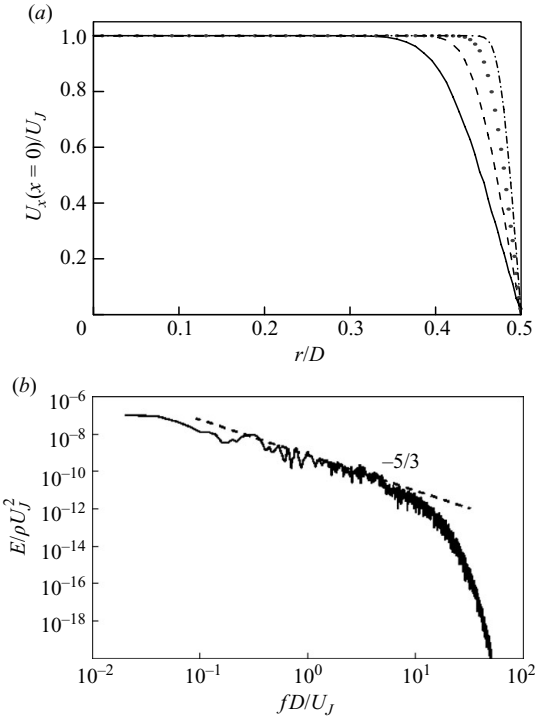

FIGURE 2. Jet inflow conditions: (*a*) axial velocity profiles: ———, $D/\theta = 50$; – – – –, 80; · · · · · · ·, 120; — · —, 180; (*b*) energy spectrum of the background disturbance. Here f is the frequency.

Re_D	D/θ	Domain size	Number of grid points
100	50, 80, 120, 180	$-3.6 < x/D < 30$, $r/D < 14$, $0 \leqslant \phi < 2\pi$	$337(x) \times 214(r) \times 32(\phi)$
3600	50, 80, 120, 180	$-3.6 < x/D < 40$, $r/D < 7$, $0 \leqslant \phi < 2\pi$	$337(x) \times 132(r) \times 64(\phi)$
10^4	50, 80, 120, 180	$-3.6 < x/D < 30$, $r/D < 7$, $0 \leqslant \phi < 2\pi$	$449(x) \times 132(r) \times 128(\phi)$
10^5	50, 80, 120, 180	$-3.6 < x/D < 18$, $r/D < 7$, $0 \leqslant \phi < 2\pi$	$545(x) \times 132(r) \times 128(\phi)$

TABLE 1. Computational domain sizes and numbers of grid points.

in the dissipation region, respectively (Pope 2000). The background disturbance is randomly distributed in space at the jet exit, and the amplitude (r.m.s. value) of the background disturbance is set to be $u_J = 0.001U_J$ at $Re_D = 100$, 3600 and 10^4, and $u_J = 0.003U_J$ at $Re_D = 10^5$, respectively, following the experimental conditions by Russ & Strykowski (1993) and Crow & Champagne (1971).

The computational domain sizes and the numbers of grid points for all the cases are given in table 1. To resolve a large velocity gradient inside the shear layer, non-uniform grids are distributed in the axial and radial directions. In the radial direction, grids are clustered in the shear layer (near $r/D = 0.5$), e.g. at least 10 grid points are located inside the initial shear layer at the jet exit. To accurately predict the shear layer evolution near the jet exit, the grids are clustered at the jet exit in the axial direction: for instance, at $Re_D = 10^5$, the grid sizes distributed from the jet exit to

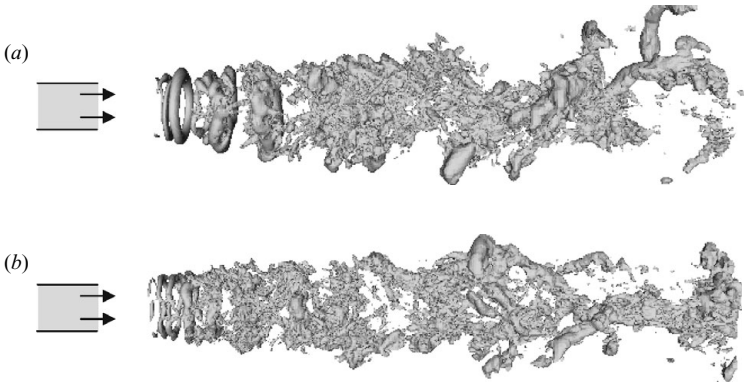

FIGURE 3. Instantaneous vortical structures at $Re_D = 10^5$ and $D/\theta = 180$: (*a*) without and (*b*) with the background disturbance ($u_J = 0.003U_J$) at the jet exit. Shown here are the iso-surfaces of pressure, $p/\rho U_J^2 = -0.03$.

nearly the end of the potential core (i.e. $x/D \simeq 4$) range from $\Delta x/D = 0.00833$ to 0.03. Uniform grids are distributed in the azimuthal direction.

To examine the validity of the background disturbance provided at the jet exit, LESs are performed in the case of $Re_D = 10^5$ and $D/\theta = 180$ with and without the disturbance. Figure 3 shows the instantaneous vortical structures for both cases. As shown, the initial growth of the shear layer is very different between two cases although the amplitude of the disturbance is fairly small; the disturbance generates small-scale vortex rings in the vicinity of the jet exit, whereas larger vortex rings are observed without the disturbance. As shown in figure 4, the present results (mean and fluctuation velocities) from LES with the disturbance agree very well with the experimental ones, indicating the adequacy of numerical parameters chosen in the present numerical simulation (see also figures 8 and 9 later in this paper). With the disturbance, the velocity fluctuations grow more rapidly very near the jet exit than those without the disturbance (see the inset in figure 4*b*). This earlier growth of shear layer produces smaller-scale vortex rings and earlier saturation of turbulence, resulting in smaller r.m.s. values and larger mean centreline velocity in downstream locations (figure 4). Further discussion on the effect of the background disturbance on the jet evolution is given in Appendix A. Unless otherwise specified, the results shown in this paper are obtained with the disturbance.

The discussions on the computational aspects concerning the quality of grid resolution and the applicability of the LES technique to the study of Reynolds-number dependence are given in Appendix B.

3. Results and discussion

3.1. *Vortical structure and near-field statistics*

Figures 5–7 show the variations of vortical structures with the jet initial momentum thickness for $Re_D = 3600$, 10^4 and 10^5, respectively. As shown, the evolution of vortical structures significantly depends on both the Reynolds number and the jet momentum thickness. For all the cases shown here, the shear layer in the vicinity of the jet exit becomes unstable due to the Kelvin–Helmholtz instability and rolls up into vortex rings downstream. For $Re_D = 3600$ (figure 5), with increasing D/θ, the vortex rings form earlier and thus large-scale vortical structures occur earlier through vortex pairing. On the other hand, when Re_D and D/θ become sufficiently large

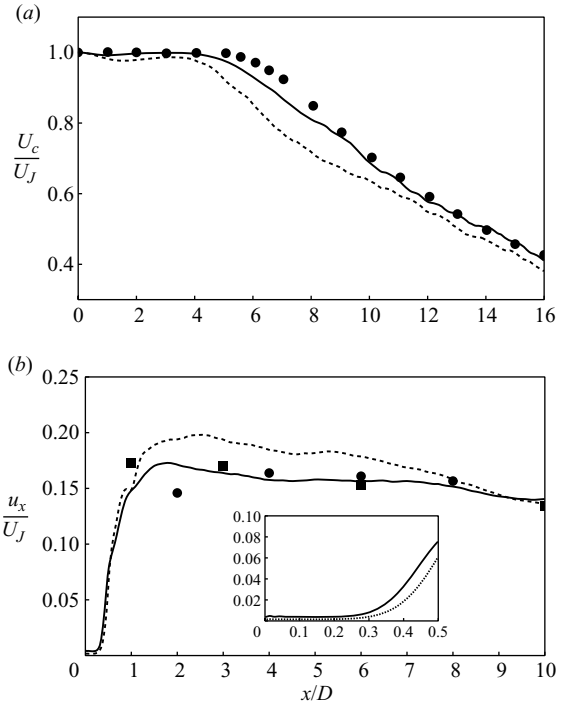

FIGURE 4. Evolutions of the mean and r.m.s. axial velocities at $Re_D = 10^5$ and $D/\theta = 180$: (*a*) mean velocity along the centreline; (*b*) r.m.s. velocity fluctuations along the shear layer ($r = 0.45D$). ———, with the disturbance ($u_J = 0.003U_J$); – – – –, without the disturbance; •, Crow & Champagne (1971) ($Re_D \approx 10^5$, $D/\theta \approx 600$ and $u_J \approx 0.003U_J$; in (*b*), $r/D \approx 0.5$); ■, Sami, Carmody & Rouse (1963) ($Re_D \approx 2.2 \times 10^5$; in (*b*), $r/D \approx 0.5$).

(e.g. at $Re_D = 10^5$ and $D/\theta = 180$), the shear layer in the vicinity of the jet exit is very thin and becomes rapidly unstable. This early growth of the shear layer leads to the saturation of the shear layer, resulting in the promotion of fine-scale vortical structures in downstream locations (figure 7*d*). As a result, a gradual inhibition of energetic large-scale structures with increasing D/θ is observed for $Re_D = 10^4$ and 10^5 in figures 6 and 7, respectively. The promotion of fine-scale structures from the saturation of the shear layer was previously observed by Zaman & Hussain (1981) from an excitation at a non-dimensional frequency of $St_\theta = f\theta/U_J = 0.017$.

Since the evolution of vortical structures is closely associated with jet mixing, the jet inflow condition such as the jet momentum thickness should be an important factor determining jet mixing. Figure 8 shows the variations of the mean axial velocity along the centreline for different Re_D and D/θ, together with previous experimental results. The jet-centreline velocity is regarded as one of the indices representing the degree of jet mixing. The flow is steady at $Re_D = 100$ but is unsteady at other Reynolds numbers. As shown in this figure, the present simulation results show excellent agreements with those by Crow & Champagne (1971), Zaman & Hussain (1981) and Cho *et al.* (1998), and a reasonable agreement with those by Russ & Strykowski (1993). For $Re_D = 100$ (steady laminar flow), the jet-centreline velocity decays more rapidly at lower D/θ through the molecular diffusion. At high Reynolds numbers at which the flows are unsteady, the interaction between the vortical structures and the ambient flow plays an important role in jet mixing. For $Re_D = 3600$, the jet-centreline

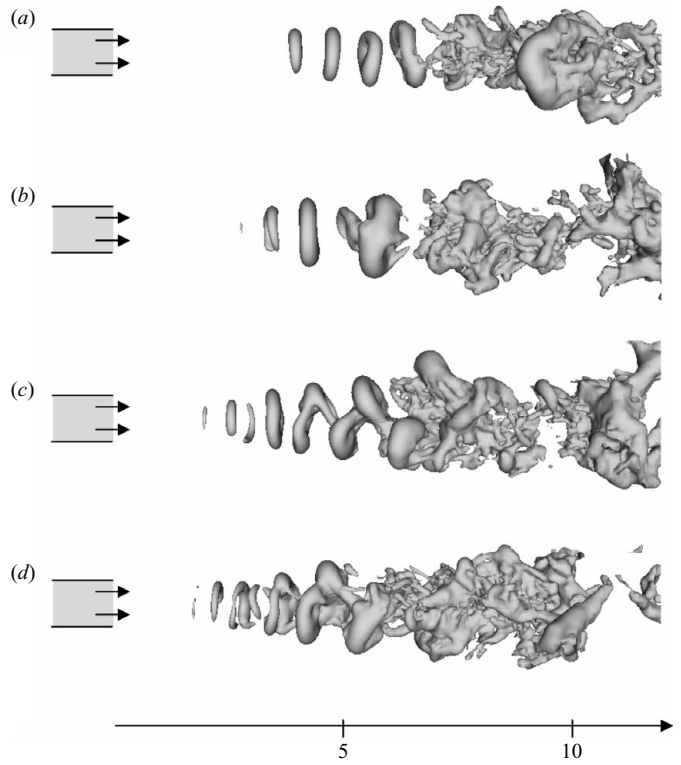

FIGURE 5. Instantaneous vortical structures at $Re_D = 3600$: (*a*) $D/\theta = 50$; (*b*) 80; (*c*) 120; (*d*) 180. Shown here are the iso-surfaces of pressure, $p/\rho U_J^2 = -0.03$.

velocity decreases more rapidly at higher D/θ (figure 8*b*). This more rapid decay at higher D/θ is attributed to the earlier occurrence of large-scale structures as shown in figure 5. On the contrary, for $Re_D = 10^5$, the jet-centreline velocity decreases more slowly at higher D/θ (figure 8*d*). This is because at higher D/θ earlier saturation of the shear layer instability results in fine-scale vortical structures at downstream locations and decreases jet mixing. The reduction of jet mixing due to the promotion of fine-scale vortical structures was reported by Zaman & Hussain (1981). For $Re_D = 10^4$ (figure 8*c*), the variation of the jet-centreline velocity with D/θ shows an intermediate behaviour between those for $Re_D = 3600$ and 10^5. That is, at low D/θ ($\leqslant 80 - 120$), the jet-centreline velocity decreases more rapidly with increasing D/θ, but it decreases more slowly with increasing D/θ at high D/θ ($\geqslant 80 - 120$). This behaviour is consistent with the vortical evolutions shown in figure 6.

Figure 9 shows the variations of the r.m.s. axial velocity fluctuations along the centreline for $Re_D = 3600$, 10^4 and 10^5, together with previous experimental results. The present results show good agreements with the experimental data. Again, the jet inflow condition significantly changes the evolution of the r.m.s. axial velocity fluctuations. For $Re_D = 3600$, the r.m.s. axial velocity fluctuations grow more quickly at higher D/θ. In contrast, the r.m.s. axial velocity fluctuations for $Re_D = 10^5$ increase much more slowly at higher D/θ due to the early saturation of the shear layer (see the inset in figure 9*c*), as mentioned earlier. For $Re_D = 10^4$, the variation in D/θ shows a mixed behaviour between those for $Re_D = 3600$ and 10^5.

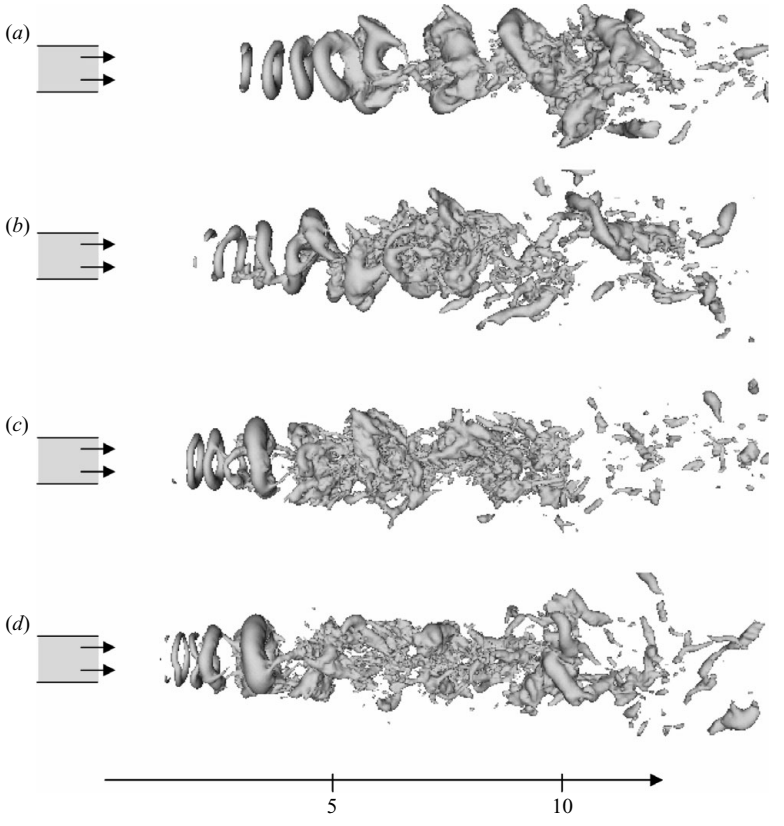

FIGURE 6. Instantaneous vortical structures at $Re_D = 10^4$: (*a*) $D/\theta = 50$; (*b*) 80; (*c*) 120; (*d*) 180. Shown here are the iso-surfaces of pressure, $p/\rho U_J^2 = -0.03$.

3.2. *Instability modes*

There exist two different flow instability modes in a jet: one is the shear layer mode that is associated with a high-frequency oscillation due to the shear layer roll-up, and the other is the jet-preferred mode that is associated with a low-frequency oscillation due to the evolution of large-scale coherent structures. It has been known that the shear layer mode has a dominant frequency at $St_\theta = f\theta/U_J \approx 0.017$ from theoretical analyses (Michalke 1964, 1965) or at $St_\theta \approx 0.012$ from experimental measurements (Zaman & Hussain 1981), whereas the jet-preferred mode ranges from $St_D = fD/U_J \approx 0.3$ to 0.6 (Gutmark & Ho 1983; Ho & Huerre 1984).

Figure 10 shows the dominant frequencies corresponding to the shear layer mode with different normalizations, together with those from previous experiments (Kibens 1980; Zaman & Hussain 1981; Tong & Warhaft 1994). Here, the dominant frequency is the peak frequency in the energy spectrum of the axial velocity fluctuations along the shear layer ($r/D = 0.5$). As clearly illustrated in figure 10(*a*), the shear layer mode frequency (St_θ) normalized by the initial momentum thickness shows a logarithmic increase with Re_θ ($St_\theta = 0.0052 \times \log_{10} Re_\theta + 0.00028$) and then reaches near $St_\theta = 0.017$ which is predicted from the inviscid instability theory. Here, $Re_\theta = U_J\theta/\nu$. Unless D/θ is too small, the shear layer mode frequency St_θ does not significantly depend on D/θ. The fact that St_θ at low Re_θ ($\sim O(10)$) is much lower than 0.017 is because the shear layer is greatly affected by the viscosity at low Re_θ. Actually,

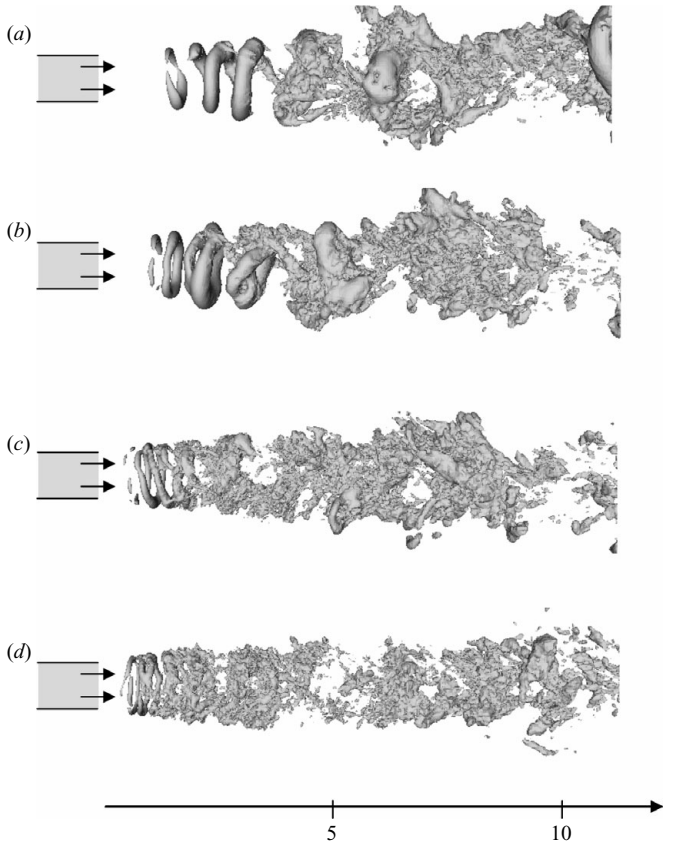

FIGURE 7. Instantaneous vortical structures at $Re_D = 10^5$: (*a*) $D/\theta = 50$; (*b*) 80; (*c*) 120; (*d*) 180. Shown here are the iso-surfaces of pressure, $p/\rho U_J^2 = -0.03$.

Villermaux (1998) investigated the instability characteristics of viscous shear layer roll-up in a mixing layer and showed that the shear layer roll-up has a lower frequency at low Re_θ than the inviscid one and then exhibits the inviscid feature with increasing Re_θ. On the other hand, as shown in figure 10(*a*), the shear layer mode frequency obtained from previous experiments is lower ($St_\theta \approx 0.012$) than $St_\theta = 0.017$ predicted by the inviscid analysis. According to Zaman & Hussain (1981), $St_\theta = 0.017$ is the frequency corresponding to the disturbances with maximum growth rate inside the shear layer, whereas $St_\theta = 0.012$ is the one corresponding to the disturbances with maximum growth. They detected $St_\theta = 0.012$ because the disturbances with maximum growth become larger than those with maximum growth rate as the jet goes downstream. Husain & Hussain (1995) mentioned that the dominance of the disturbances with maximum growth over those with maximum growth rate is attributed to the feedback mechanism from rolled-up vortices towards the jet exit. However, as shown in figure 10(*a*), the relatively lower value of $St_\theta = 0.012$ than $St_\theta = 0.017$ seems to be mainly due to the lower Re_θ ($\sim O(100)$) considered in their experiments. Thus, further experiments at high Re_θ are required to resolve this issue. On the other hand, the shear layer mode frequency normalized with the jet diameter shows much scattered behaviour (figure 10*b*), indicating that the jet diameter is not a proper length scale explaining the shear layer instability near the jet exit.

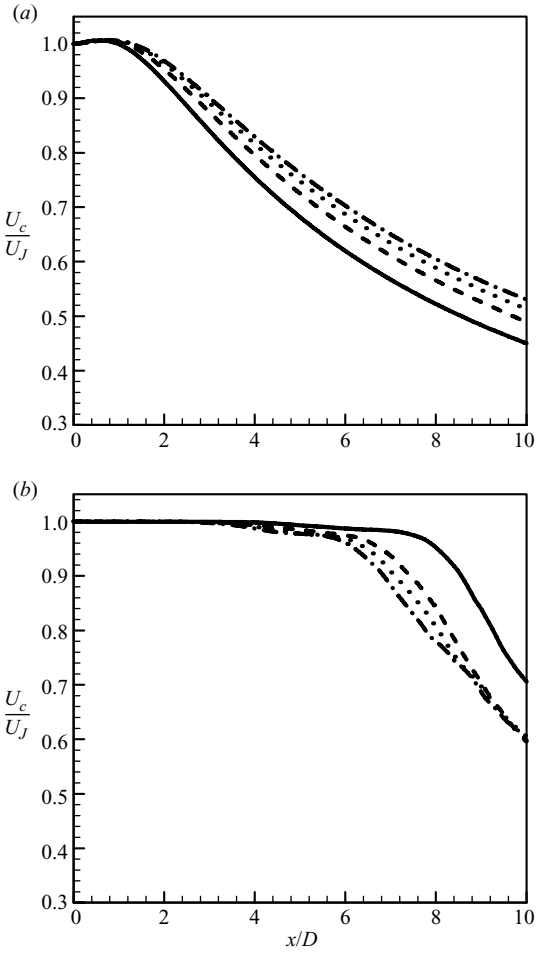

FIGURE 8. For legend see next page.

Figure 11(*a*) shows the variations of the characteristic frequency corresponding to the jet-preferred mode with the Reynolds number for different initial momentum thicknesses. The jet-preferred-mode frequency is obtained to be the peak frequency in the energy spectrum of the axial velocity fluctuations at $x/D = 4$ on the jet centreline. As shown in figure 11(*a*), the jet-preferred-mode frequency ranges from $St_D = fD/U_J \approx 0.3$ to 0.6 agreeing with the previous results (Gutmark & Ho 1983; Ho & Huerre 1984). This wide range of the characteristic frequency has been attributed to different inflow conditions (Gutmark & Ho 1983). On the other hand, it was mentioned in Ho & Huerre (1984) that with increasing Reynolds number (or with decreasing initial momentum thickness) the frequency of the jet-preferred mode increases and then approaches a constant value of about 0.42 (Drubka 1981) or 0.45 (Kibens 1981). These results suggest that the jet-preferred mode may be associated with the development of the shear layer characterized by the initial momentum thickness (Gutmark & Ho 1983).

In Crighton & Gaster (1976) and Petersen & Samet (1988), the jet-preferred mode was treated as the shear layer mode which becomes unstable near the end of the potential core (i.e. at $x/D \simeq 4$), thus being scaled with the local momentum thickness

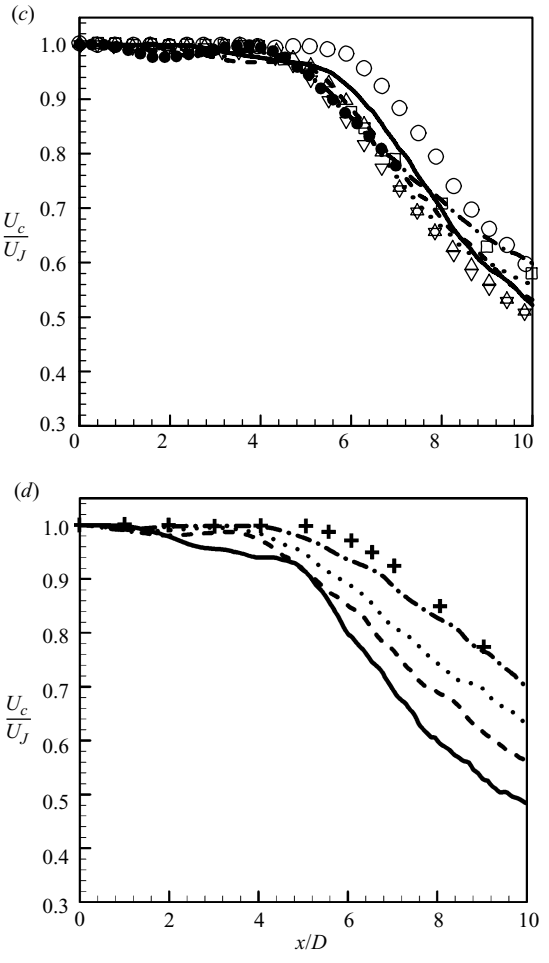

FIGURE 8. Mean axial velocity along the centreline: (*a*) $Re_D = 100$; (*b*) 3600; (*c*) 10^4; (*d*) 10^5. ———, $D/\theta = 50$; – – – –, 80; · · · · · · ·, 120; — · —, 180; ○, △, ▽, Russ & Strykowski (1993) ($D/\theta \simeq 48$, 86 and 110, respectively, for $Re_D = 10^4$ and $u_J \simeq 0.001U_J$); □, Zaman & Hussain (1981) ($D/\theta \simeq 120$ for $Re_D \approx 2 \times 10^4$ and $u_J \simeq 0.003U_J$); •, Cho *et al.* (1998) ($D/\theta \simeq 200$ for $Re_D \approx 2 \times 10^4$ and $u_J \simeq 0.003U_J$); +, Crow & Champagne (1971) ($D/\theta \approx 600$ for $Re_D \simeq 10^5$ and $u_J \simeq 0.003U_J$).

of the shear layer (θ_s) and the local centreline velocity (U_c) at that position. Crighton & Gaster (1976) showed from a theoretical approach that $f\theta_s/U_c \simeq 0.054$, and Petersen & Samet (1988) reported from their experiment that $f\theta_s/U_c \simeq 0.063$. In figure 11(*b*), when the local Reynolds number ($Re_l = U_c\theta_s/\nu$ at $x/D = 4$) is small, the frequency corresponding to the jet-preferred mode normalized by θ_s and U_c is smaller than 0.054 or 0.063. However, when the local Reynolds number becomes large ($Re_l > O(10^3)$), the jet-preferred-mode frequency shows a reasonable agreement with their values (figure 11*b*) although it is much higher for the cases of $Re_D = 10^4$ and $D/\theta = 180$ and $Re_D = 10^5$ and $D/\theta = 120$. The result shown in this figure indicates that when the local Reynolds number is large, the coherent structures may be understood as a kind of the shear layer mode as argued by Crighton & Gaster (1976) and Petersen & Samet (1988). On the other hand, concerning the jet-preferred mode existing distinct from the shear layer mode (Jendoubi & Strykowski 1994), a caution should be given to the

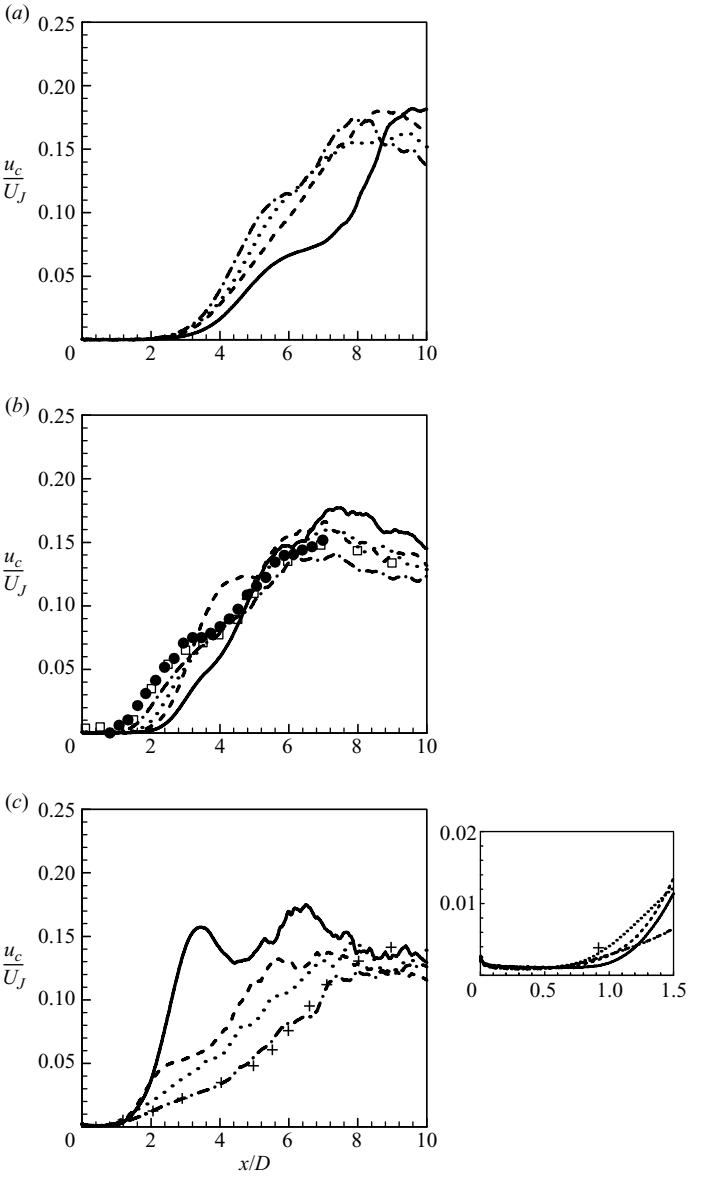

FIGURE 9. r.m.s. axial velocity fluctuations along the centreline: (*a*) $Re_D = 3600$; (*b*) 10^4; (*c*) 10^5. ———, $D/\theta = 50$; – – – –, 80; · · · · · · ·, 120; — · —, 180; □, Zaman & Hussain (1981) ($D/\theta \simeq 120$ for $Re_D \approx 2 \times 10^4$ and $u_J \simeq 0.003U_J$); •, Cho *et al.* (1998) ($D/\theta \simeq 200$ for $Re_D \approx 2 \times 10^4$ and $u_J \simeq 0.003U_J$); +, Crow & Champagne (1971) ($D/\theta \approx 600$ for $Re_D \simeq 10^5$ and $u_J \simeq 0.003U_J$).

study of the variation of jet-preferred-mode frequency with the inflow conditions. In the context of the hydrodynamic stability theory, the jet-preferred mode is understood as a global mode of marginally stable flow that is sensitive to external forcing (Huerre & Monkewitz 1990). So, when a certain disturbance is close to the receptivity band of the jet, the corresponding mode may be amplified rather than the jet-preferred mode (Hussain 1986). As a typical example, when the jet-preferred-mode frequency is near to that corresponding to the nth pairing of an initial shear layer instability, the

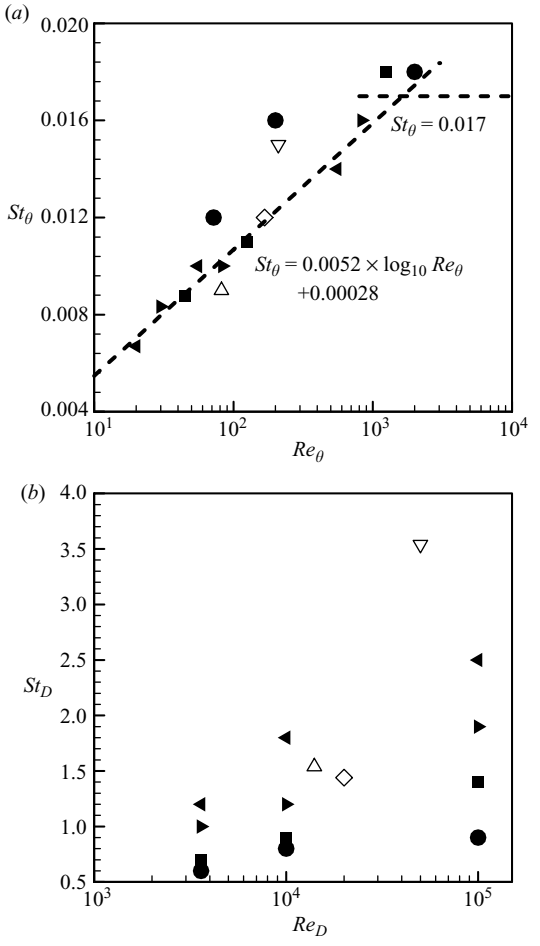

FIGURE 10. Shear layer mode: (*a*) St_θ; (*b*) St_D. •, $D/\theta = 50$; ■, 80; ►, 120; ◄, 180. The frequencies corresponding to the shear layer mode are obtained from the energy spectra of the axial velocity along the shear layer ($r/D = 0.5$) at different axial locations in $0.5 \leqslant x/D \leqslant 2$ depending on the Reynolds number and D/θ. Here, ▽, Kibens (1980) ($Re_D = 5 \times 10^4$ and $D/\theta \approx 240$); ◇, Zaman & Hussain (1981) ($Re_D = 2 \times 10^4$ and $D/\theta \approx 120$); △, Tong & Warhaft (1994) ($Re_D = 1.4 \times 10^4$ and $D/\theta \approx 170$).

coherent structure may result from subharmonic sequence starting at the jet nozzle instead of the jet-preferred mode. In the present study, the cases of $D/\theta = 50$ and 80 at $Re_D = 10^4$ belong to this situation. Since the detail of background disturbances at the jet exit affects whether coherent structures result from the pairing of an initial shear layer instability or not, it is difficult to seek truly universal scaling of the jet-preferred mode. Therefore, further studies with control of background disturbances should be conducted to resolve this issue. In this respect, studies on excited jets may provide some directions towards the universal scaling of the jet-preferred mode, as suggested by Hussain & Zaman (1981) and Hussain (1986).

3.3. *Mode analysis*

The vortical structures in a jet can be decomposed into disturbances corresponding to Fourier components with the azimuthal wavenumbers m. The disturbances corresponding to $m = 0$, 1 and 2 are called axisymmetric (mode 0), helical (mode 1)

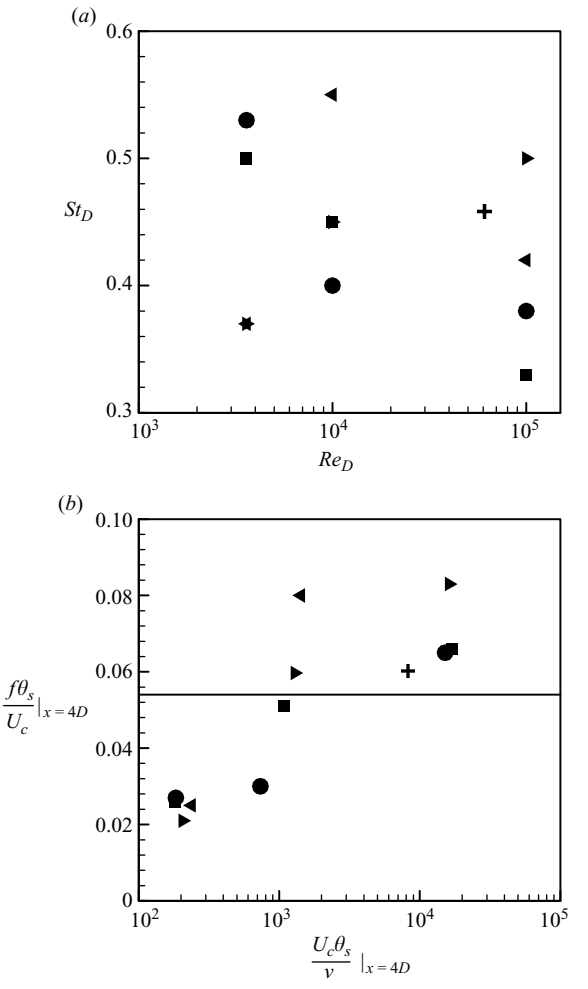

FIGURE 11. Jet-preferred mode: (*a*) St_D; (*b*) $f\theta_s/U_c|_{x=4D}$. •, $D/\theta = 50$; ■, 80; ►, 120; ◄, 180. The frequencies corresponding to the jet-preferred mode are obtained from the energy spectra of the axial velocity at $x/D = 4$ on the jet centreline. In (*b*), U_c and θ_s are the jet-centreline velocity and momentum thickness measured at $x/D = 4$, respectively. The solid line in (*b*) denotes the theoretical value of 0.054 predicted by Crighton & Gaster (1976), and + denotes the value measured by Petersen & Samet (1988) ($Re_D = 5.6 \times 10^4$).

and double-helix (mode 2) modes, respectively. Batchelor & Gill (1962) first analysed the dominant azimuthal modes of a structure existing in a circular jet and showed that all azimuthal modes become theoretically unstable near the jet exit but mode 0 grows fastest, whereas past the potential core only mode 1 is unstable. The dominance of mode 1 past the potential core was also predicted by Michalke & Hermann (1982). Then, Cohen & Wygnanski (1987) and Raman, Rice & Reshotko (1994) experimentally measured properties of each modal structure such as the amplification rate and the relative amplitude in the region close to the shear layer. Their results were consistent with those of the previous theoretical studies. Recently, Jung, Garmard & George (2004) and Gamard, Jung & George (2004) argued that mode 0 has the largest energy only in the near-field region and mode 2 is the dominant mode of coherent structures in the downstream location ($x/D \gtrsim 6$). The difference among these previous

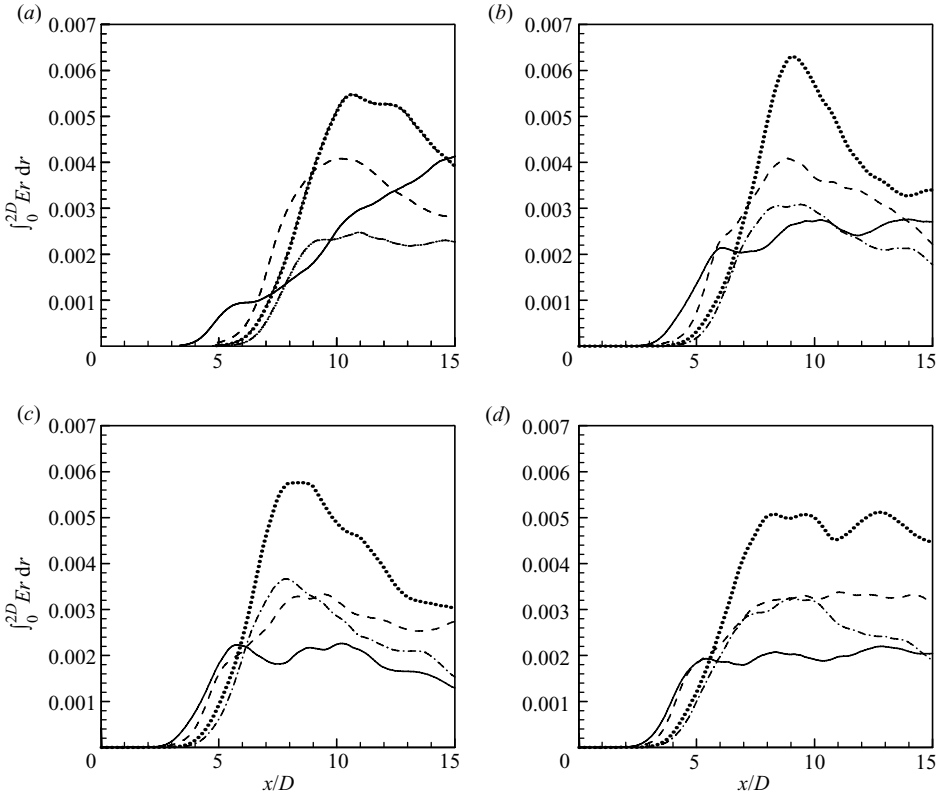

FIGURE 12. Growth of the integrated energy of axial velocity fluctuations along the axial direction at $Re_D = 3600$: (*a*) $D/\theta = 50$; (*b*) 80; (*c*) 120; (*d*) 180. ———, mode 0; – – – –, mode 1; · · · · · · ·, mode 2; — · —, mode 3.

results has not been clearly resolved. It may be associated with different Reynolds numbers and jet initial conditions adopted in the previous studies, because they significantly change the vortical evolutions as shown in the present study. Therefore, it should be interesting to see how these modes evolve downstream depending on the initial momentum thickness and Reynolds number using the present simulation data.

Figures 12–14 show the energy of the axial velocity fluctuations integrated over $0 \leqslant r \leqslant 2D$ at each azimuthal mode, $\widetilde{E}(x, m)(=\int_0^{2D} E(x, r, m) r \mathrm{d}r)$, for different initial momentum thicknesses at $Re_D = 3600$, 10^4 and 10^5, respectively. As is shown later, the energy at $r/D > 2$ is almost zero, so its contribution is negligible. The energy of axial velocity fluctuations at each azimuthal wavenumber is obtained from

$$E(x, r, m) = \overline{\hat{u}'_x(x, r, m, t)\hat{u}'_x(x, r, m, t)^*}, \tag{3.1}$$

where $\hat{u}'_x(x, r, m, t)$ is the Fourier coefficient of axial velocity fluctuations, * denotes the complex conjugate and the overbar denotes the averaging in time. As shown in figures 12–14, the evolution of each azimuthal mode along the axial direction depends on both Re_D and D/θ. Near the jet exit, the axisymmetic mode (mode 0) is dominant regardless of the Reynolds number, but becomes less dominant as D/θ increases. At $Re_D = 3600$ and $D/\theta = 50$, mode 0 grows gradually in the axial direction. However, with increasing D/θ, mode 0 has a local peak near the end of the potential core, and then is almost unchanged or slightly decays. The peak occurs slightly earlier as

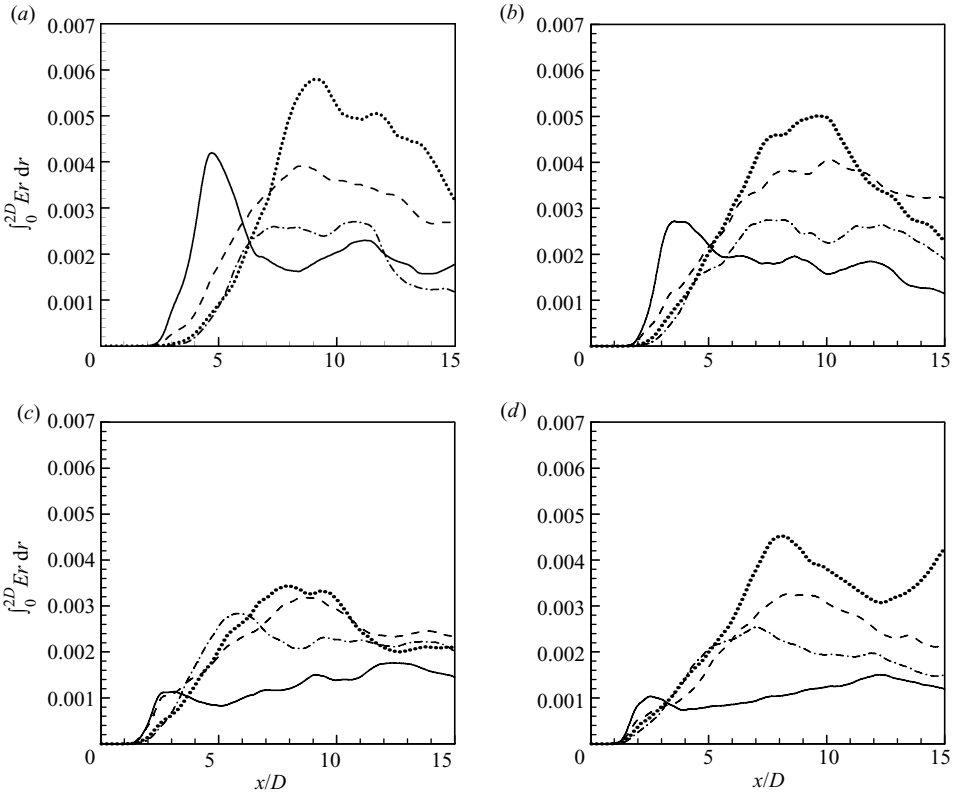

FIGURE 13. Growth of the integrated energy of axial velocity fluctuations in the axial direction at $Re_D = 10^4$: (*a*) $D/\theta = 50$; (*b*) 80; (*c*) 120; (*d*) 180. ———, mode 0; – – – –, mode 1; · · · · · · ·, mode 2; — · —, mode 3.

D/θ increases. With increasing Reynolds number, the dominance of mode 0 near the jet exit becomes weak, although mode 0 still remains dominant at $x/D \lesssim 5$ for relatively thick shear rates such as $D/\theta = 50$ and 80 at $Re_D = 10^4$ and $D/\theta = 50$ at $Re_D = 10^5$. In particular, for the cases of $D/\theta = 120$ and 180 at $Re_D = 10^5$, other modes grow faster than mode 0 even within the potential core, not to mention further downstream. It is interesting to note that the growth of mode 0 in the axial direction is significantly suppressed with increasing Reynolds number. The decay of mode 0 and the growth of higher modes are supported by the fact that the vortex rings become weak and less organized with increasing D/θ as shown in figures 5–7.

On the other hand, the evolutions of azimuthal modes downstream of the potential core are more complicated. Nevertheless, overall, mode 2 is dominant in downstream locations, which agrees with the proper orthogonal decomposition (POD) results of Freund & Colonius (2002) ($Re_D = 3600$) and Jung *et al.* (2004) ($Re_D = 78\,400$, 117 600 and 156 800). With increasing Reynolds number, however, the dominance of mode 2 becomes relatively weak as the integrated energies of mode 1 and mode 3 become comparable to that of mode 2. Especially, for the case of $D/\theta = 50$ and $Re_D = 10^5$, mode 1 is most dominant in the downstream location ($x/D > 5$). This weaker dominance of mode 2 at higher Reynolds numbers can also be found by comparing the results from Jung *et al.* (2004) and Freund & Colonius (2002). On the other hand, the downstream evolutions of modes look similar between $D/\theta = 120$

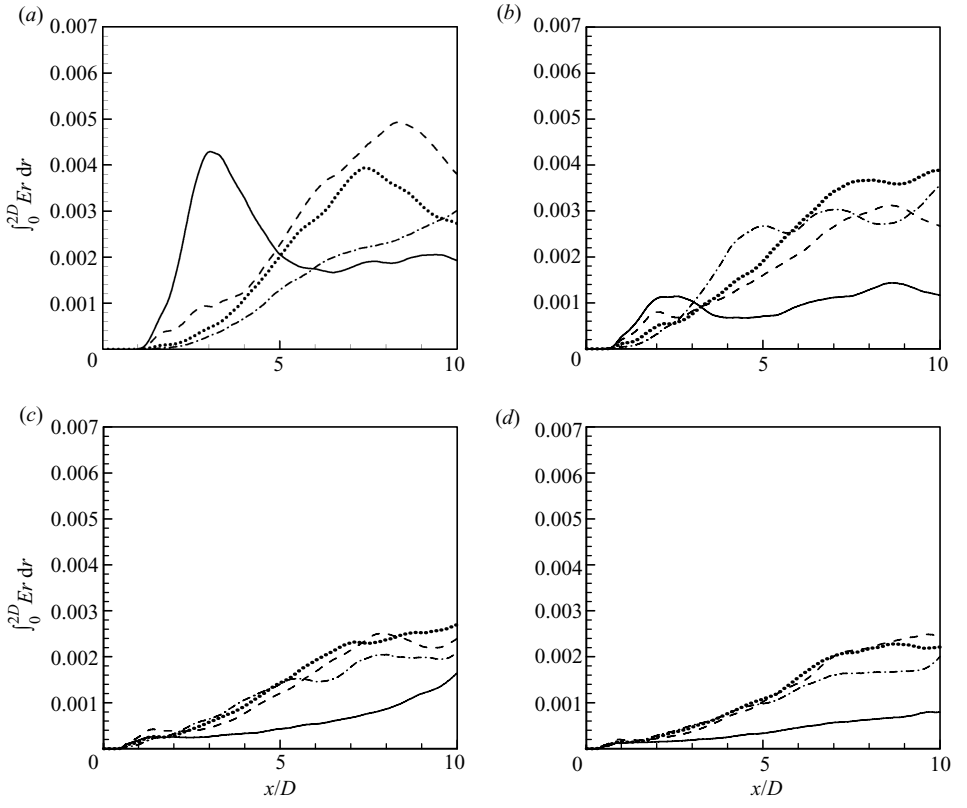

FIGURE 14. Growth of the integrated energy of axial velocity fluctuations along the axial direction at $Re_D = 10^5$: (*a*) $D/\theta = 50$; (*b*) 80; (*c*) 120; (*d*) 180. ———, mode 0; – – – –, mode 1; · · · · · · ·, mode 2; — · —, mode 3.

and 180 at $Re_D = 10^5$, indicating that the modal structures are relatively insensitive to the initial momentum thickness at high Reynolds numbers once the initial shear layer is sufficiently thin.

So far, we considered the evolution of azimuthal modes of integrated axial velocity fluctuations ($0 \leqslant r \leqslant 2D$). Since the evolution of azimuthal modes significantly depends on the shear rate of the initial shear layer, we investigate the growth of azimuthal modes along the shear layer. The profiles of $E(r, m)$ at a few different axial locations are drawn in figures 15 and 16 for the cases of $D/\theta = 50$ and 180 ($Re_D = 10^4$), respectively. Near the jet exit, disturbances grow along the shear layer. For $D/\theta = 50$, mode 0 grows much faster than other modes (figures 15*a* and 15*b*). However, for $D/\theta = 180$, all the modes considered here grow almost simultaneously near the jet exit. On the other hand, in downstream locations ($x/D = 6$ and 8), modes 1 and 2 become dominant along the radial direction. More specifically (for example, at $x/D = 8$), mode 1 is dominant at $0.2 \leqslant r/D \leqslant 0.5 \sim 0.6$, whereas mode 2 is dominant at 0.5–$0.6 \leqslant r/D \leqslant 1$–$1.5$. However, near the centreline, mode 0 is most dominant even at farther downstream locations. Similar profiles of $E(r, m)$ are also observed in downstream locations for $Re_D = 3600$ and 10^5 (not shown here). Therefore, the characteristics of $E(r, m)$ in downstream locations exhibit the following behaviour irrespective of the jet inflow condition, i.e. the dominant mode changes from mode 0 near the centreline to mode 1 and then to mode 2 with increasing radial direction. It

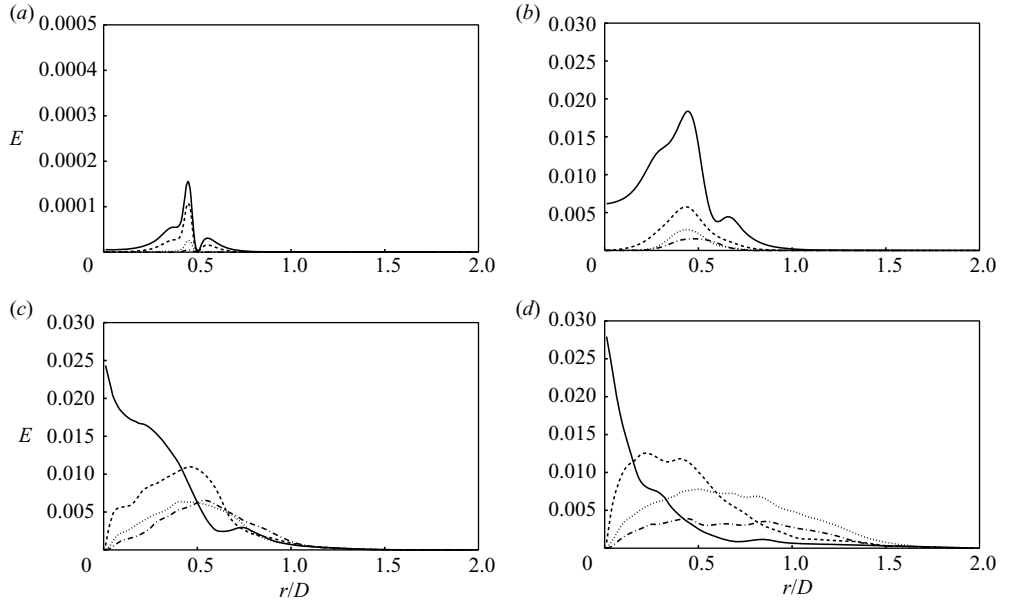

FIGURE 15. Radial distribution of the energy of axial velocity fluctuations at $Re_D = 10^4$ and $D/\theta = 50$: (*a*) $x/D = 2$; (*b*) 4; (*c*) 6; (*d*) 8. ———, mode 0; – – – –, mode 1; · · · · · · ·, mode 2; — · —, mode 3.

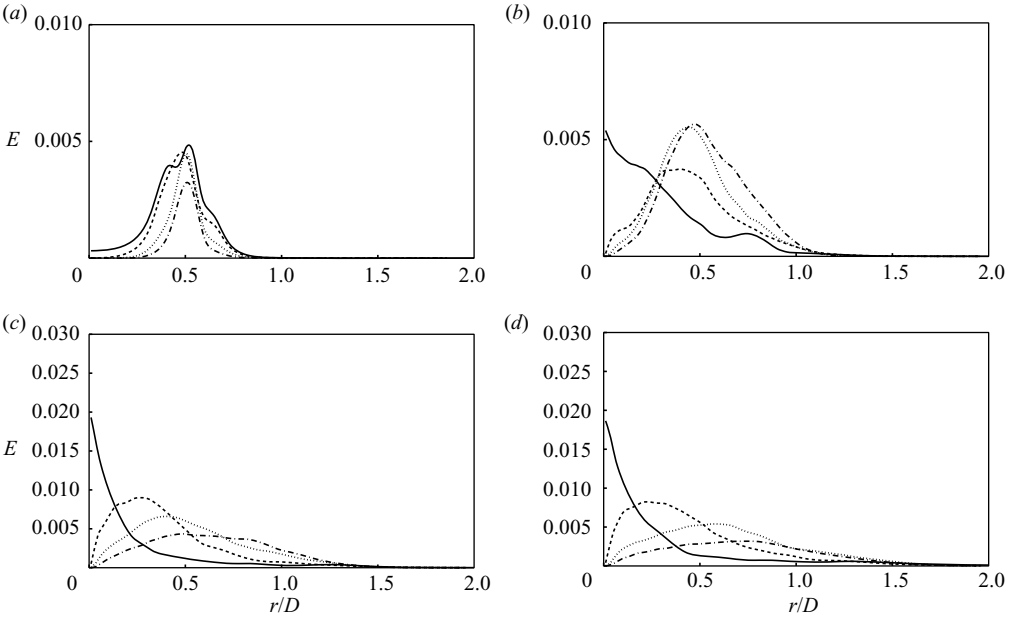

FIGURE 16. Radial distribution of the energy of axial velocity fluctuations at $Re_D = 10^4$ and $D/\theta = 180$: (*a*) $x/D = 2$; (*b*) 4; (*c*) 6; (*d*) 8. ———, mode 0; – – – –, mode 1; · · · · · · ·, mode 2; — · —, mode 3.

is important to note that the large energy level of mode 2 in downstream locations observed in figures 12–14 results from the dominance of mode 2 at large r/D (and thus larger area), implying that the effect of mode 2 on the vortical evolution in view of the energy integrated over the domain may be overemphasized.

4. Conclusions

In the present study, the effects of the jet inflow conditions such as the initial momentum thickness (θ) and the background disturbances on the downstream evolution of a circular jet were investigated using LES. We considered four different initial momentum thicknesses, $D/\theta = 50$, 80, 120 and 180, and three different Reynolds numbers, $Re_D = U_J D/\nu = 3600$, 10^4 and 10^5, where U_J is the jet inflow velocity and D is the jet diameter.

The present study showed that the flow characteristics of the circular jet significantly change with the initial momentum thickness, and the effect of the initial momentum thickness also depends on the Reynolds number. As a result, the important features of the jet such as mixing and turbulence intensity were very sensitive to these conditions. For all the Reynolds numbers considered in this study, the vortex rings were generated at an earlier axial location with decreasing initial momentum thickness. In the case of relatively low Reynolds numbers like $Re_D = 3600$, this early growth of shear layer with decreasing initial momentum thickness generated large-scale coherent structures in earlier downstream locations, resulting in the mixing enhancement and an increase in turbulence intensity. However, at a high Reynolds number of $Re_D = 10^5$, the early growth of the shear layer led to the occurrence of fine-scale structures through the saturation of shear layer and resulted in the reduction of mixing and turbulence intensity with decreasing initial momentum thickness.

The jet initial momentum thickness changed the temporal instability of the jet such as the shear layer and jet-preferred modes. The shear layer frequency normalized by the initial momentum thickness and jet inflow velocity increased logarithmically with the Reynolds number, $St_\theta \sim \log_{10} Re_\theta$, and reached near 0.017 predicted from the inviscid instability theory. Unless D/θ was too small, the shear layer mode frequency St_θ did not significantly depend on D/θ. On the other hand, the characteristic frequency corresponding to the jet-preferred mode depended on the Reynolds number and the initial momentum thickness. When the Reynolds number based on the centreline velocity and shear layer thickness at $x/D = 4$ was large enough, the jet-preferred-mode frequency was reasonably scaled with the local momentum thickness and the jet-centreline velocity. Therefore, the diversity of the jet-preferred-mode frequency reported in the literature may be caused by the different evolution processes of the shear layer depending on the jet inflow conditions.

A mode analysis was conducted to investigate how the disturbances evolve according to the initial momentum thickness and Reynolds number. In this analysis, the vortical structures were decomposed into the azimuthal modes. In view of the energy of the axial velocity fluctuations integrated over $0 \leqslant r/D \leqslant 2$, double-helix mode (mode 2) became dominant past the potential core, whereas near the jet exit the axisymmetric mode (mode 0) was dominant. In view of the local energy, the disturbances grew along the shear layer near the jet exit: for thick shear layer, mode 0 grew much faster than other modes, but modes 0–3 grew almost simultaneously for thin shear layer. However, past the potential core, the dominant mode changed from mode 0 near the centreline to mode 1 and then to mode 2 with increasing radial direction regardless of the initial shear layer thickness.

In the present simulation, we have shown how the downstream evolution of the jet is affected by the jet inflow conditions characterizing the evolution of the initial shear layer. One of the conclusions drawn in the present study is that the shear layer and jet-preferred-mode frequencies, when appropriately non-dimensionalized, have tendencies to asymptotically approach constant values as the Reynolds number increases. It may be interesting to see if this conclusion is still valid for $Re_D > 10^5$ at which the jet

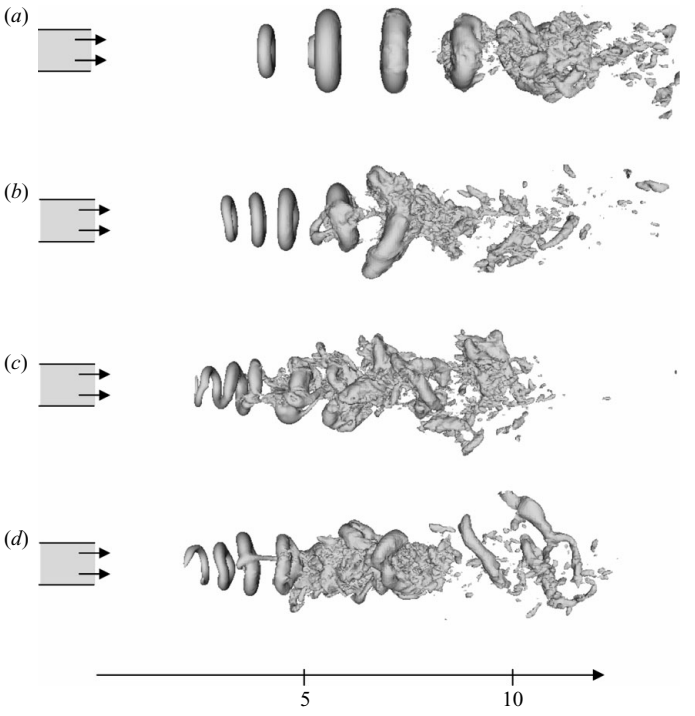

FIGURE 17. Instantaneous vortical structures at $Re_D = 10^4$ and $D/\theta = 50$: (*a*) $u_J/U_J = 0$; (*b*) 0.001; (*c*) 0.005; (*d*) 0.01. Shown are the iso-pressure surfaces of $p/\rho U_J^2 = -0.03$.

inflow boundary layer is turbulent. Hill *et al.* (1976) and Crighton (1981) mentioned that the jet characteristics significantly change depending on whether the state of the jet inflow is laminar or turbulent. Cooper & Crighton (2000) conjectured that the characteristics of coherent structures may change as the Reynolds number increases over $O(10^5)$. Therefore, the instability characteristics in a very high-Reynolds-number jet should be an important subject to be investigated.

The self-similarity feature of the jet has been regarded as one of the important issues (Wygnanski & Fielder 1969; Dowling & Dimotakis 1990). An issue that is not covered in the present study is how the self-similar solution of the jet depends on the jet inflow conditions. Although there have been a few interesting studies in this direction such as George (1989), Hussein, Capp & George (1994) and Boersma, Brethouwer & Nieuwstadt (1998), a systematic investigation on the effect of the jet inflow conditions, covering wide ranges of the Reynolds number and the jet initial momentum thickness, on the self-similar solution should be another important topic to pursue.

This work is supported by the National Research Laboratory Program of the Korean Ministry of Science and Technology through KOSEF.

Appendix A. Effect of the background disturbance level on the jet evolution

The level of background disturbances at the jet exit is known to play an important role in the vortical evolution in a circular jet. In this appendix, we examine how the background disturbance level affects the jet evolution at $Re_D = 10^4$. We consider two different initial momentum thicknesses, $D/\theta = 50$ and 180, representing thick and

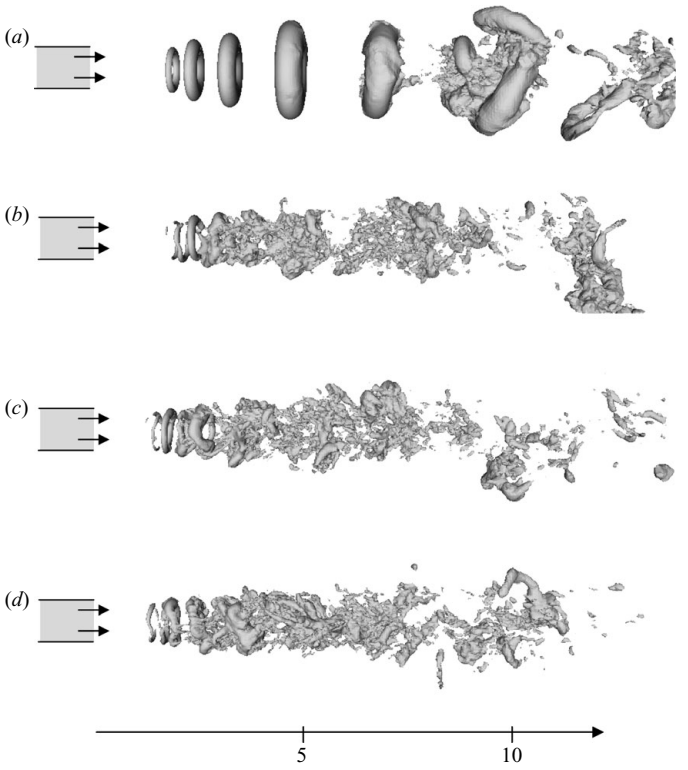

FIGURE 18. Instantaneous vortical structures at $Re_D = 10^4$ and $D/\theta = 180$: (*a*) $u_J/U_J = 0$; (*b*) 0.001; (*c*) 0.005; (*d*) 0.01. Shown are the iso-pressure surfaces of $p/\rho U_J^2 = -0.03$.

thin shear layers, respectively. For each initial momentum thickness, three different background disturbance levels, $u_J/U_J = 0.001, 0.005$ and 0.01, are imposed.

Figures 17 and 18 show the instantaneous vortical structures for different background disturbance levels at $D/\theta = 50$ and 180, respectively. Without disturbances, strong axisymmetric vortex rings occur for both thick and thin shear layers and persist farther downstream. With background disturbances, however, vortex rings become smaller and less organized. As shown in these figures, both the background disturbance level and the initial momentum thickness significantly change the evolution of vortical structures. The influence of background disturbance level is weaker for $D/\theta = 180$ than for $D/\theta = 50$. For the thick shear layer ($D/\theta = 50$), vortex rings are generated earlier with increasing disturbance level. On the other hand, for the thin shear layer ($D/\theta = 180$), vortex rings appear at nearly the same axial location irrespective of the level of disturbances, suggesting that, for thin shear layer, small amount of disturbances is enough to trigger the shear layer evolution and the jet statistics do not change much with the level of disturbances.

Figures 19 and 20 show the variations of the mean axial velocity and r.m.s. axial velocity fluctuations along the centreline for different background disturbance levels at $D/\theta = 50$ and 180, respectively. Similar to the vortical structures, the effect of background disturbance level is more evident for the thick shear layer ($D/\theta = 50$) than for the thin one ($D/\theta = 180$). Especially, the difference in the mean velocities with and without background disturbance is much larger at $D/\theta = 50$ than at $D/\theta = 180$. At $D/\theta = 50$, the jet-centreline velocity decays much more slowly

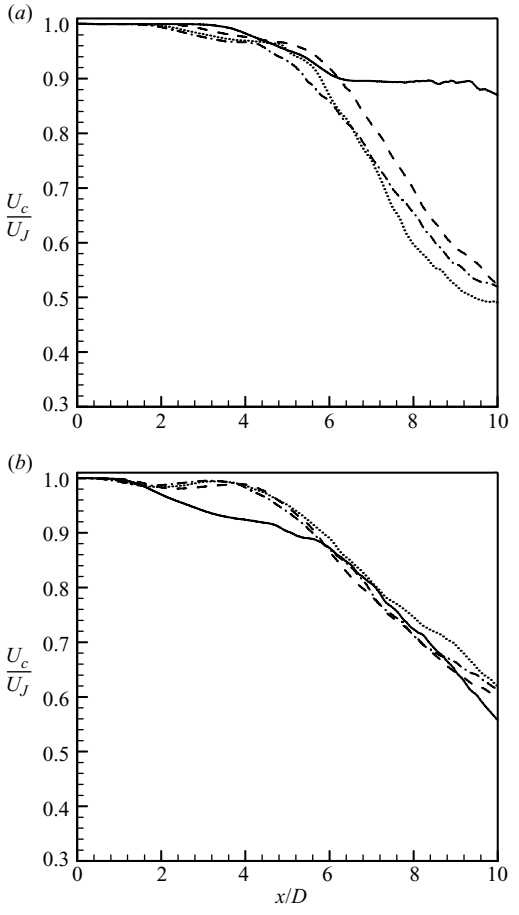

FIGURE 19. Mean axial velocity along the centreline ($Re_D = 10^4$): (*a*) $D/\theta = 50$; (*b*) 180. ———, $u_J/U_J = 0$; – – – –, 0.001; · · · · · · ·, 0.005; — · —, 0.01.

without the background disturbance than with the disturbance (figure 19*a*). The r.m.s. axial velocity fluctuations grow more quickly near the jet exit at higher background disturbance level, but the fluctuations saturate earlier with the background disturbance (figure 20*a*). Note that the r.m.s. value with $u_J = 0$ becomes very large due to the large-scale structures existing there. On the contrary, for $D/\theta = 180$ (figures 19*b* and 20*b*), the mean axial velocity and r.m.s. axial velocity fluctuations are very similar among themselves when background disturbances are provided. Without the background disturbances, the r.m.s. axial velocity fluctuations become very large in downstream locations because of the large-scale structures formed there (figure 18*a*).

Appendix B. Quality of grid resolution and applicability of LES technique to the study of Reynolds-number dependence

In this appendix, we address the quality of grid resolution adopted in our LES, and the applicability of LES technique to the study of Reynolds-number dependence. To check the grid resolution in the axial direction, we increase and decrease the minimum grid spacing $\Delta x_{min}/D$ from 0.0167 to 0.0333 and 0.00833, respectively, and show the results in figure 21(*a*). As shown, further reduction in $\Delta x_{min}/D$ does not

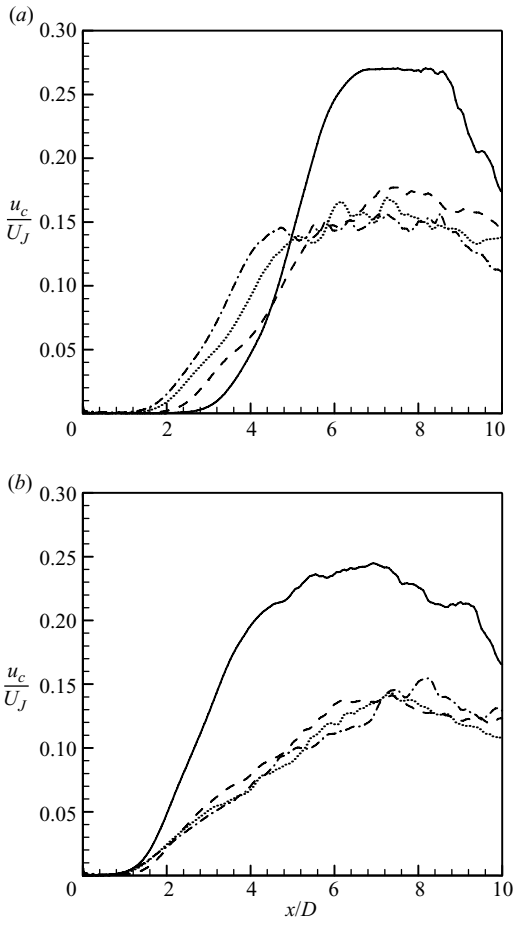

FIGURE 20. r.m.s. axial velocity fluctuations along the centreline ($Re_D = 10^4$): (*a*) $D/\theta = 50$; (*b*) 180. ———, $u_J/U_J = 0$; – – – –, 0.001; · · · · · · ·, 0.005; — · —, 0.01.

change the solution. The same result is also obtained for the r.m.s. velocity fluctuations (not shown in this paper). Similarly, we change the grid resolution in the azimuthal direction and present the results in figure 21(*b*). Little change is observed even with doubling the grid spacing, showing the appropriateness of grid resolution adopted in our simulation. Figure 22 shows the contours of instantaneous ν_t/ν for different grid resolutions, where $\nu_t = c\Delta^2|\tilde{S}|$ is the SGS eddy viscosity, Δ is the filter width (grid size), $\tilde{S} = \sqrt{2\tilde{S}_{ij}\tilde{S}_{ij}}$ and c is obtained from a dynamic procedure (Germano *et al.* 1991; Lilly 1992). In the case of coarse grid resolution, large values of ν_t are observed even very near the jet exit although the initial shear layer is not turbulent. With proper grid resolution, ν_t is very small there. Therefore, it is clear that coarse grids distributed in the initial shear layer region result in unrealistic ν_t and wrong evolution of shear layer.

Now, let us discuss the applicability of LES technique to the study of Reynolds-number dependence. In this paper, we presented the r.m.s. velocity fluctuations obtained from the resolved velocity fields for three different Reynolds numbers. In other words, the contribution from SGS velocity fluctuations was not included. Thus, we examine the magnitude of the SGS kinetic energy to investigate whether or not

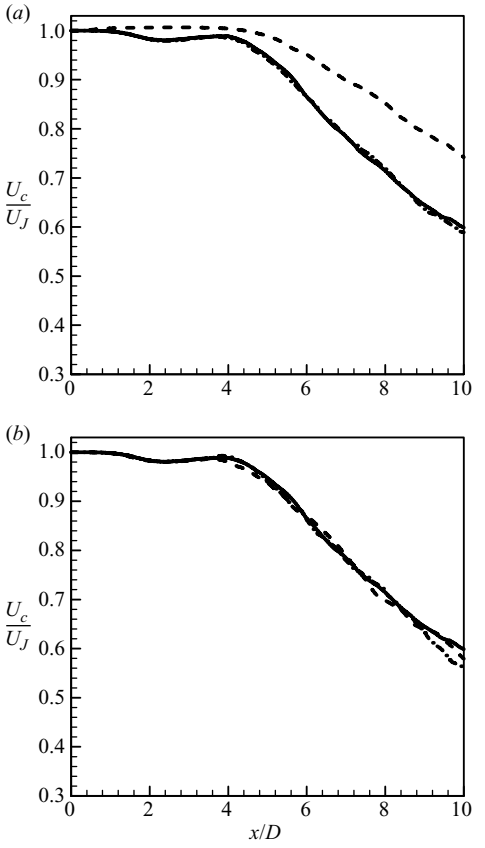

FIGURE 21. Resolution study for the case of $Re_D = 10^4$ and $D/\theta = 180$: (*a*) axial grid resolution (– – – –, $\Delta x_{min}/D = 0.0333$; ———, 0.0167 (original resolution); — · —, 0.00833); (*b*) azimuthal grid resolution (– – – –, $\Delta\phi/2\pi = 1/64$; ———, 1/128 (original resolution); — · —, 1/256).

neglecting the SGS contribution to the Reynolds stresses is justified. The SGS kinetic energy may be obtained from the model proposed by Vreman, Geurts & Kuerten (1994) and Vreman (2004): $k_\tau = 2\nu_t|\tilde{S}|$. The ratio of SGS kinetic energy to the resolved kinetic energy averaged over the azimuthal direction and time is shown in figure 23 for $\mathrm{Re}_D = 10^5$ and $D/\theta = 180$. The maximum value is only about 5%, indicating that the turbulent kinetic energy would be little changed even after the SGS kinetic energy is included. Figure 24 shows the ratio of SGS kinetic energy to the resolved kinetic energy averaged over the azimuthal direction from an instantaneous flow field. The value of this ratio is smaller than 0.2 even for $\mathrm{Re}_D = 10^5$, which implies that the present LES is well resolved (Pope 2000). The SGS dissipation is obtained from $-\boldsymbol{\tau}_{ij}\tilde{S}_{ij}$ and its ratio to the viscous dissipation $\nu\tilde{S}_{ij}\tilde{S}_{ij}$ is shown in figure 25. The SGS dissipation is much larger than the viscous dissipation and becomes more significant at larger Reynolds number. Therefore, it seems clear with the present grid resolution that, as the Reynolds number increases, the SGS dissipation becomes much bigger than the viscous dissipation, but the SGS kinetic energy remains small and thus the resolved kinetic energy alone properly represents the total turbulent kinetic energy.

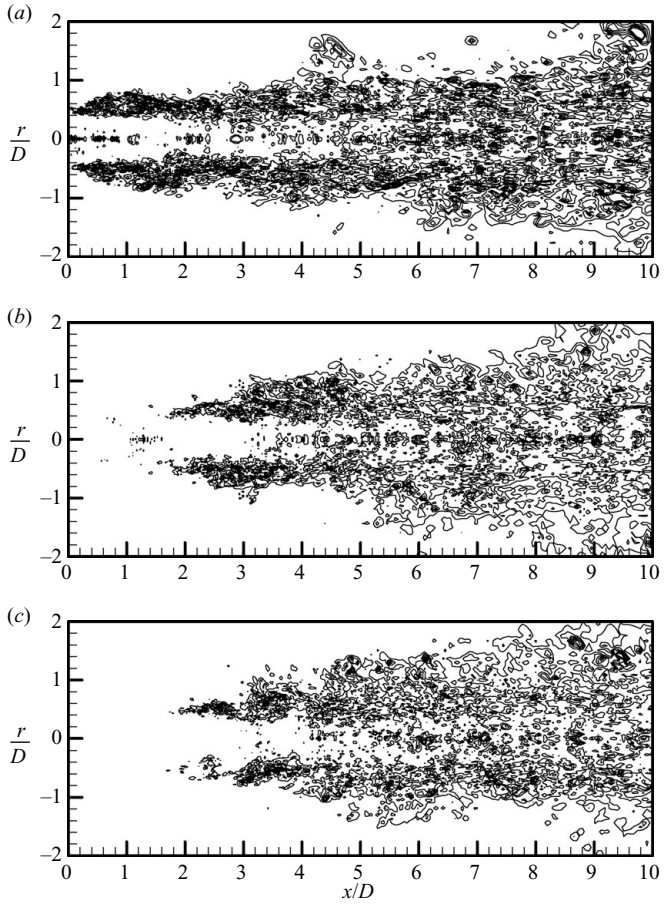

FIGURE 22. Ratio of instantaneous eddy viscosity to the molecular viscosity at $Re_D = 10^4$ and $D/\theta = 180$ in the case of axial grid resolution: (*a*) coarse grid resolution; (*b*) original grid resolution; (*c*) fine grid resolution. Contour levels are from −1 to 3 by increments of 0.5. Negative values are dashed.

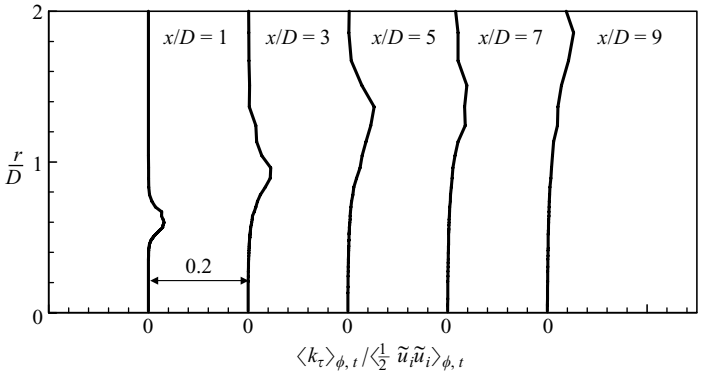

FIGURE 23. Ratio of SGS kinetic energy to the resolved kinetic energy, $\langle k_\tau \rangle_{\phi,t} / \langle \frac{1}{2} \tilde{u}_i \tilde{u}_i \rangle_{\phi,t}$, at $Re_D = 10^5$ and $D/\theta = 180$.

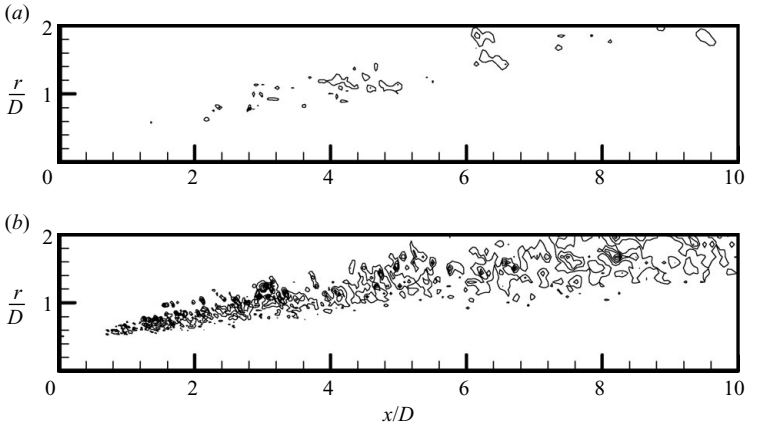

FIGURE 24. Ratio of SGS kinetic energy to the resolved kinetic energy, $\langle k_\tau \rangle_\phi / \langle \frac{1}{2} \tilde{u}_i \tilde{u}_i \rangle_\phi$, for $D/\theta = 180$: (*a*) $Re_D = 10^4$; (*b*) 10^5. Contour levels are from -0.2 to 0.2 by increments of 0.02. Negative values are dashed.

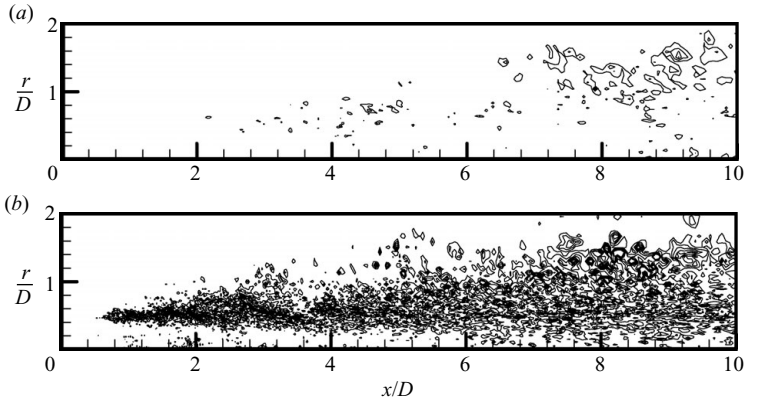

FIGURE 25. Ratio of SGS dissipation to the viscous dissipation, $\langle -\tau_{ij} \tilde{S}_{ij} \rangle_\phi / \langle \nu \tilde{S}_{ij} \tilde{S}_{ij} \rangle_\phi$, from an instantaneous field for $D/\theta = 180$: (*a*) $Re_D = 10^4$; (*b*) 10^5. Contour levels are from -1 to 15 by increments of 1. Negative values are dashed.

REFERENCES

AKSELVOLL, K. & MOIN, P. 1996 An efficient method for temporal integration of the Navier–Stokes equations in confined axisymmetric geometries. *J. Comput. Phys.* **125**, 454–463.

BABU, P. C. & MAHESH, K. 2004 Upstream entrainment in numerical simulations of spatially evolving round jets. *Phys. Fluids* **16**, 3699–3705.

BATCHELOR, G. K. & GILL, A. E. 1962 Analysis of the stability of axisymmetric jets. *J. Fluid Mech.* **14**, 529–551.

BODONY, D. J. & LELE, S. K. 2005 On using large-eddy simulation for the prediction of noise from cold and heated turbulent jets. *Phys. Fluids* **17**, 085103.

BOERSMA, B. J., BRETHOUWER, G. & NIEUWSTADT, F. T. M. 1998 A numerical investigation on the effect of the inflow conditions on the self-similar region of a round jet. *Phys. Fluids* **10**, 899–909.

BOGEY, C. & BAILLY, C. 2005 Effects of inflow conditions and forcing on subsonic jet flows and noise. *AIAA J.* **43**, 1000–1007.

BRADSHAW, P. 1966 The effect of initial conditions on the development of a free shear layer. *J. Fluid Mech.* **26**, 225–236.

Cho, S. K., Yoo, J. Y. & Choi, H. 1998 Vortex pairing in an axisymmetric jet using two-frequency acoustic forcing at low to moderate Strouhal numbers. *Exp. Fluids* **25**, 305–315.

Cohen, J. & Wygnanski, I. 1987 The evolution of instabilities in the axisymmetric jet. Part 1. The linear growth of disturbances near the nozzle. *J. Fluid Mech.* **176**, 191–219.

Cooper, A. J. & Crighton, D. G. 2000 Global modes and superdirective acoustic radiation in low-speed axisymmetric jets. *Eur. J. Mech.* B – *Fluids* **19**, 559–574.

Crighton, D. G. 1981 Acoustics as a branch of fluid mechanics. *J. Fluid Mech.* **106**, 261–298.

Crighton, D. G. & Gaster, M. 1976 Stability of slowly diverging jet flow. *J. Fluid Mech.* **77**, 397–413.

Crow, S. C. & Champagne, F. H. 1971 Orderly structure in jet turbulence. *J. Fluid Mech.* **48**, 547–591.

Dowling, D. R. & Dimotakis, P. E. 1990 Similarity of the concentration field of gas-phase turbulent jets. *J. Fluid Mech.* **218**, 109–141.

Drubka, R. E. 1981 Instabilities in near field of turbulent jets and their dependence on initial conditions and Reynolds number. PhD dissertation, Illinois Institute of Technology, Chicago.

Freund, J. B. & Colonius, T. 2002 POD analysis of sound generation by a turbulent jet. *AIAA paper* 2002-0072.

Gamard, S., Jung, D. & George, W. K. 2004 Downstream evolution of the most energetic modes in a turbulent axisymmetric jet at high Reynolds number. Part 2. The far-field region. *J. Fluid Mech.* **514**, 205–230.

George, W. K. 1989 Self-preservation of turbulent flows and its relation to initial conditions and coherent structures. In *Advances in Turbulence*. Springer.

Germano, M., Piomelli, U., Moin, P. & Cabot, W. H. 1991 A dynamic subgrid-scale eddy viscosity model. *Phys. Fluids* A **3**, 1760–1765.

Gutmark, E. & Ho, C.-M. 1983 Preferred modes and the spreading rates of jets. *Phys. Fluids* **26**, 2932–2938.

Hill Jr., W., Jenkins, R. C. & Gilbert, B. L. 1976 Effects of the initial boundary-layer state on turbulent jet mixing. *AIAA J.* **14**, 1513–1514.

Ho, C.-M. & Huerre, P. 1984 Perturbed free shear layers. *Annu. Rev. Fluid Mech.* **16**, 365–424.

Huerre, P. & Monkewitz, P. A. 1990 Local and global instabilities in spatially developing flows. *Annu. Rev. Fluid Mech.* **22**, 473–537.

Husain, H. S. & Hussain, F. 1995 Experiments on subharmonic resonance in a shear layer. *J. Fluid Mech.* **304**, 343–372.

Hussain, A. K. M. F. 1983 Coherent structures – reality and myth. *Phys. Fluids* **26**, 2816–2850.

Hussain, A. K. M. F. 1986 Coherent structures and turbulence. *J. Fluid Mech.* **173**, 303–356.

Hussain, A. K. M. F. & Zaman, K. B. M. Q. 1981 The 'preferred mode' of the axisymmetric jet. *J. Fluid Mech.* **110**, 39–71.

Hussain, A. K. M. F. & Zedan, M. F. 1978a Effects of the initial condition on the axisymmetric free shear layer: effects of the initial momentum thickness. *Phys. Fluids* **21**, 1100–1112.

Hussain, A. K. M. F. & Zedan, M. F. 1978b Effects of the initial condition on the axisymmetric free shear layer: effects of the initial fluctuation level. *Phys. Fluids* **21**, 1475–1481.

Hussein, H. J., Capp, S. P. & George, W. K. 1994 Velocity measurements in a high-Reynolds-number, momentum-conserving, axisymmmetric, turbulent jet. *J. Fluid Mech.* **258**, 31–75.

Jendoubi, S. & Strykowski, P. J. 1994 Absolute and convective instability of axisymmetric jets with external flow. *Phys. Fluids* **6**, 3000–3009.

Jung, D., Garmard, S. & George, W. K. 2004 Downstream evolution of the most energetic modes in a turbulent axisymmetric jet at high Reynolds number. Part 1. The near-field region. *J. Fluid Mech.* **514**, 173–204.

Kibens, V. 1980 Discrete noise spectrum generated by an acoustically excited jet. *AIAA J.* **18**, 434–441.

Kibens, V. 1981 The limit of initial shear layer influence on jet development. *AIAA paper* 81-1960.

Lee, S., Lele, S. K. & Moin, P. 1992 Simulation of spatially evolving turbulence and the applicability of Taylor's hypothesis in compressible flow. *Phys. Fluids* A **4**, 1521–1530.

Lilly, D. K. 1992 A proposed modification of the Germano subgrid-scale closure method. *Phys. Fluids* A **4**, 633–635.

Mi, J., Nobes, D. S. & Nathan, G. J. 2001 Influence of jet exit conditions on the passive scalar field of an axisymmetric free jet. *J. Fluid Mech.* **432**, 91–125.

Michalke, A. 1964 On the inviscid instability of the hyperbolic tangent velocity profile. *J. Fluid Mech.* **19**, 543–556.

Michalke, A. 1965 On spatially growing disturbances in an inviscid shear layer. *J. Fluid Mech.* **23**, 521–544.

Michalke, A. & Hermann, G. 1982 On the inviscid instability of a circular jet with external flow. *J. Fluid Mech.* **114**, 343–359.

Petersen, R. A. & Samet, M. M. 1988 On the preferred mode of jet instability. *J. Fluid Mech.* **194**, 153–173.

Pope, S. B. 2000 *Turbulent Flows*. Cambridge University Press.

Raman, G., Rice, E. J. & Reshotko, E. 1994 Mode spectra of natural disturbances in a circular jet and the effect of acoustic forcing. *Exp. Fluids* **17**, 415–426.

Russ, S. & Strykowski, P. J. 1993 Turbulent structure and entrainment in heated jets: the effect of initial conditions. *Phys. Fluids* A **5**, 3216–3225.

Sami, S., Carmody, T. & Rouse, H. 1963 Jet diffusion in the region of flow establishment. *J. Fluid Mech.* **27**, 231–252.

Stanley, S. A. & Sarkar, S. 2000 Influence of nozzle conditions and discrete forcing on turbulent planar jets. *AIAA J.* **38**, 1615–1623.

Tong, C. & Warhaft, Z. 1994 Turbulence suppression in a jet by means of a fine ring. *Phys. Fluids* **6**, 328–333.

Villermaux, E. 1998 On the role of viscosity in shear instabilities. *Phys. Fluids* **10**, 368–373.

Vreman, A. W. 2004 An eddy-viscosity subgrid-scale model for turbulent shear flow: algebraic theory and applications. *Phys. Fluids* **16**, 3670–3681.

Vreman, B., Geurts, B. & Kuerten, H. 1994 Realizability conditions for the turbulent stress tensor in large eddy simulation. *J. Fluid Mech.* **278**, 351–362.

Wygnanski, I. & Fielder, H. 1969 Some measurements in the self-preserving jet. *J. Fluid Mech.* **38**, 577–612.

Yule, A. J. 1978 Large-scale structure in the mixing layer of a round jet. *J. Fluid Mech.* **89**, 413–432.

Zaman, K. B. M. Q. 1985 Far-field noise of a subsonic jet under controlled excitation. *J. Fluid Mech.* **152**, 83–111.

Zaman, K. B. M. Q. & Hussain, A. K. M. F. 1981 Turbulence suppression in free shear flows by controlled excitation. *J. Fluid Mech.* **103**, 133–159.